Unraveling the Mechanism of the Persistent Photoconductivity in InSe and its doped counterparts

Liping Liao, Evgeniya Kovalska, Jan Luxa, Lukáš Dekanovsky, Vlastimil Mazanek, Lukáš Valdman, Bing Wu, Štěpán Huber, Martin Mikulics, Zdenek Sofer**

L. Liao, Dr. E. Kovalska, Dr. J. Luxa, L. Dekanovsky, Dr. V. Mazanek, L. Valdman, B. Wu, Dr. S. Huber, Prof. Z. Sofer
Department of Inorganic Chemistry, University of Chemistry and Technology
Technicka 5, 166 28, Prague, Czech Republic
E-mail: soferz@vscht.cz; liaol@vscht.cz

Dr. E. Kovalska
College of Engineering Mathematics and Physical Sciences, University of Exeter
EX4 4QF, Exeter, United Kingdom

Dr. M. Mikulics
Ernst Ruska-Centre (ER-C-2), Forschungszentrum Jülich, D-52425 Jülich, Germany

Dr. M. Mikulics
Jülich-Aachen Research Alliance, Fundamentals of Future Information Technology, D-52425 Jülich, Germany

Keywords: InSe, Persistent Photoconductivity, Doping, Photodetectors, Two-dimensional

Abstract

Dopant levels in layered compound InSe have considerable potential in optoelectronic devices. Dopant-induced trap states are essential in determining the optoelectrical properties of semiconductors. However, detailed studies of the persistent photoconductivity (PPC) and related mechanism in doped InSe are still not available. Here, we systematically investigated the dependence of excitation energy on the shallow donor level caused by the dopants (Ge, Sn) in InSe. Notably, prolonger decay time originates from extrinsic Ge, Sn dopants and these doping-assisted states improve the optoelectrical performance of pristine InSe. Sn-doped InSe single crystal device can achieve a maximum responsivity of around 1.7×10^6 A W^{-1} under red light, a relatively higher external quantum efficiency (EQE) of 3.2×10^6 % and detectivity of 6.18×10^{13} Jones. In addition, Hall measurements identify the carrier concentration and hall mobility of pristine InSe are significantly changed by Ge and Sn dopants. We demonstrate that doping Ge, Sn atoms is responsible for the obvious photoconductivity and beneficial for the

high-performance photodetector, offering intriguing opportunities for novel holographic memory applications.

1. Introduction

The photodetector has proved to be advanced optoelectronic functionalities in sensors, logic circuits, and communication systems.[1] The amplitude, sensitivity, responsivity, and spectral responsivity play important roles in the photodetection capability of photodetector for converting light into electrical signals.[2] Interaction between light and matter in optoelectronic devices based on the basic principle of photo-related excitation, for example, photogenerated electron-hole pairs separate and then transport, entering into the conduction band and valence band, respectively. The absorbed light is output in the form of photocurrent. In this process, dopant states in semiconductor photoconductors are essential in determining photoexcited carriers' properties, like lifetime, mobility, activation energy.[3]-[7] The presence of dopant states may prolong the response time due to re-excitation from trapped (shallow level/deep level) states into the conduction or valence band.[8] So, trap states should be studied in depth to regulate their properties to balance the photodetector's sensitivity and response time. Usually, except for inherent defects/native vacancies, dopant from the extrinsic element is regarded as an impurity, which may introduce various types of trapped states.

As for electronic application, doping is a straightforward strategy for modulating the Fermi level of a semiconductor,[9][10] achieving *p*- or *n*-channel material. So far, several experimental studies have shown that transition metal atom doping, such as Fe, Co, or Ni could affect the electronic and magnetic properties of two-dimensional (2D) semiconductors due to the change of band structure modification and mass fluctuation after doping.[11] Among these 2D materials, layered III-VI compound indium selenide (InSe) has drawn extensive attention owing to its remarkable electronic and optoelectronic properties. Impurity and dopants in InSe play an important role in potential photoelectronic applications.[12],[13] Elements of groups IV and V possibly function as amphoteric impurities in InSe. While few studies are accessible to the optical and electrical properties of InSe doped with group IV atoms.

Recently, high photoresponsivity,[14] photoconductivity, photovoltaic effect[15] and thermoelectric effect[16] have been reported in InSe-based photodetectors and phototransistors. However, detailed optoelectronic studies on these InSe-based devices of persistent photoconductivity (PPC) and the relevant mechanism is still not available. PPC is a sustained conductivity phenomenon after photon irradiation is terminated,[17]-[19] which is stems from the

trap states or impurities in the semiconductor. Moreover, the PPC effect modifies carrier transport properties, a promising strategy to explore light-induced memory applications, such as storage-class memory, resistive computing, and neuromorphic computing. Therefore, it is essential to understand the PPC effect to control carriers transfer in the InSe materials family.

In this study, we obtained high-quality Ge-doped InSe (InSe(Ge)) and Sn-doped InSe (InSe(Sn)) single crystals grown by crystallization from In-Se melt in quartz ampoule. Here, we present a systematic study of optoelectronic properties, photoconductivity based on bulk InSe crystals and Ge-, Sn-doped InSe crystals photodetector. The effects of dopant (Ge, Sn) in InSe crystal have been investigated by measuring the PPC dependence on various photon doses and the excitation energy. The results are observed to fit well to the stretched exponential model. Large persistent photoconductivity was observed in InSe(Ge) and InSe(Sn) samples at room temperature. A series of experimental results further confirm that the Ge, Sn dopant form shallow donor levels inside the bandgap, in which the lower recapture rate or photo-induced carriers induce persistent photoconductivity. Besides, InSe(Sn)-based photodetectors achieve higher responsivity and EQE, and more than 10 times larger detectivity as compared with conventional transition-metal dichalcogenides (TMDs) materials. In addition, Hall effect was measured to characterize the hall mobility and carrier concentration of pristine InSe, InSe(Ge) and InSe(Sn), in which both InSe(Ge) and InSe(Sn) present increased Hall mobility with a significant decrease in the carrier concentration compared to the pristine InSe. Our results demonstrate effective Ge, Sn doping in InSe for higher performance photodetector and offer a novel functionality for InSe-based optoelectronic devices.

2. Results and discussion

The layered crystal structure of InSe(Ge) and InSe(Sn) (**Figure 1**a) with lattice constants a = b = 4.00 Å and c = 24.94 Å similar to that of InSe. Since each Se atom bonds with neighboring three In atoms, each Se accepts 2 valance electrons from neighboring In atoms. The optical image of the fabricated device and active channel width is shown in Figure 1b. **Figure S1** shows the optical photography of synthesized bulk pure InSe crystal, InSe(Ge) crystal and InSe(Sn) crystal. The pure InSe, InSe(Ge) and InSe(Sn) crystals were grown by the Bridgman technique as detailed in the Experimental Section. The dopant concentration in the grown crystals was revealed by inductively coupled plasma optical emission spectrometry (ICP-OES) measurements, namely 0.1% Ge and 0.1% Sn were successfully doped. The X-ray diffraction (XRD) pattern (Figure 1c) show that the prominent planes (003), (006), (015), (009), (0012)

and (0018) correspond to diffraction peaks at 11.01°, 21.68°, 31.50°, 32.58°, 43.90° and 67.88°. The strong diffraction peak at 31.5° confirms the rhombohedral phase of the InSe crystal. We note that no phase separation is observed after Ge, Sn doping into InSe, and high preferential oriented (00l) planes are observed. Raman spectrum recorded the structural characterization of the as-growth crystals with a frequency range from 70 to 300 cm^{-1} (Figure 1d). The intense Raman peaks centered at 115.4, 178.9, and 227.5 cm^{-1} correspond to the non-resonant Raman vibrational phonon modes A^1_{1g}, E^1_{2g}, and A^2_{1g}, confirming the InSe.[20] No peak shift was observed in the in-phase In-In bond stretching vibration (A^1 phonon mode) and In-In bond bending vibration (E mode), which means a small amount of Ge, Sn doping has no detectable effect on InSe lattice vibration. Scanning electron microscopy (SEM) photographs of pure InSe, InSe(Ge), and InSe(Sn) morphologies are shown in **Figure S2**. All the materials present layer-stacked microstructure. And the presence of In, Sn, Ge and Se elements, as well as their homogeneous distribution, have been verified by energy-dispersive X-ray mapping (EDS-mapping) (**Figure S3**, Supporting Information).

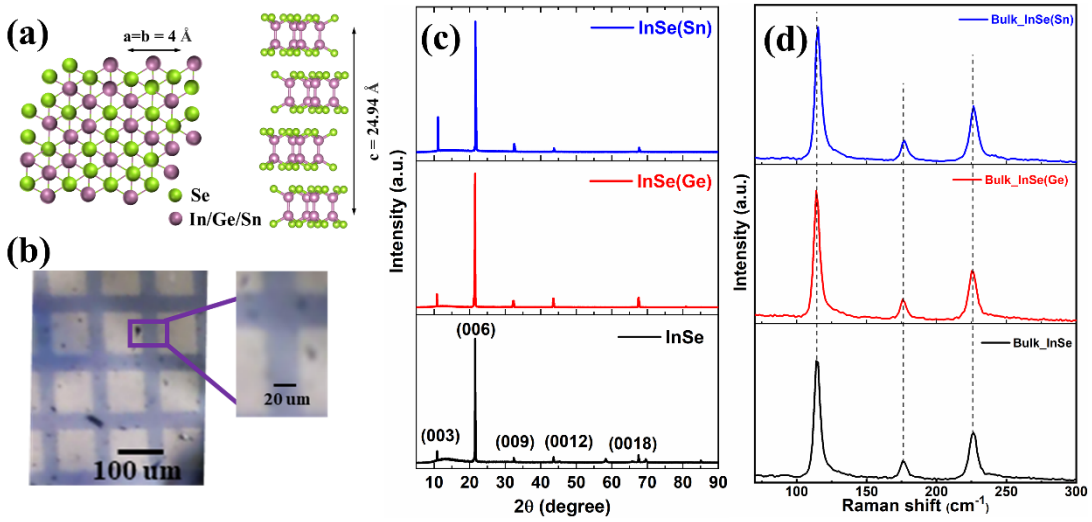

Figure 1. (a) Crystal structure of the as-grown InSe (Ge/Sn) single crystal. (b) Optical image of InSe (Ge/Sn)-based photodetector. (c) X-ray diffraction pattern of pure InSe, InSe(Ge) and InSe(Sn). (d) Raman spectra of pure InSe, InSe(Ge) and InSe(Sn).

The information about the light absorbance property of pure InSe, InSe(Ge) and InSe(Sn) was studied using UV-Vis absorption spectroscopy, shown in **Figure 2**a. The inset image shows the Tauc relation $(\alpha h\nu)^2 = A(h\nu - E_g)$ used to calculate the optical bandgap of the corresponding crystal. Here, α is the absorption coefficient, A is a constant characteristic for the material, and $h\nu$ is photon energy.[21] The bandgap values were found to be 2.3 eV, 2.21 eV and 2.17 eV for

pure InSe, InSe(Ge) and InSe(Sn). The strong PL peak (Figure 2b) is located at 1.26 eV for the cases of pure InSe and doped InSe, matching with the previous report.[22] Noted that PL peaks have obvious redshift for these three samples compared with the optical bandgap extracted from UV-Vis absorption spectra, which may originate from the native In and Se vacancies within the bandgap. Indeed, there are also the cases here,[23][24] demonstrating that the vacancies or impurities in semiconductors lead to the abovementioned redshift. The PL intensity and full width at half-maximum (FWHM) of the PL peaks are also presented in Figure 2c. The PL peak intensity of the Sn doped sample increases almost 2.5 times compared with the pure InSe. The longer carrier lifetime of Ge, Sn doped samples results in a stronger PL intensity and narrow FWHM, which signifies the reduction of photo-induced carriers non-radiative recombination.

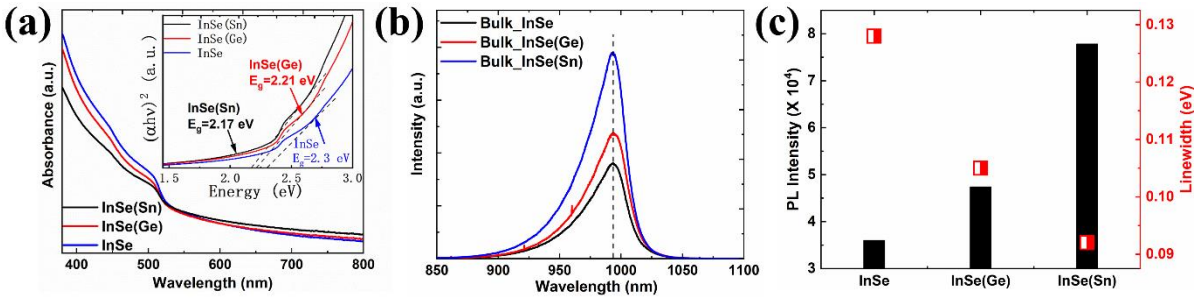

Figure 2. Optical characterization of pure InSe, InSe(Ge) and InSe(Sn). (a) UV-Vis absorption spectra, inserted: Tauc's plot; (b) PL spectra; (c) PL intensity and full width at half-maximum (FWHM).

The schematic of the band structure of semiconductors (undoped and doped ones) is shown in **Figure 3**. Extrinsic impurities inside the bandgap usually act as trap states or recombination centers. Photoexcited carriers captured by these deep/shallow traps or defects normally cause PPC. In contrast to the band-to-band recombination, PPC extends the decay time of the optoelectrical device because electrons/holes are re-trapped before combination, in which the re-trapped rate depends on the position of localized states in the bandgap. Here, ionization energy is defined as minimum kinetic energy for captured carriers to escape the impurity level. A detailed comparison for pure InSe, InSe(Ge) and InSe(Sn) corresponding electrical properties is listed in **Table1**.[25]-[27]

Table 1. Electrical properties of undoped, InSe(Ge) and InSe(Sn).

Material	N_a ($10^{15}cm^{-3}$)	N_d ($10^{15}cm^{-3}$)	$E_c - E_d$ (eV)

Pure InSe	0.4	2.6	0.027
Ge-doped InSe	1.5	32	0.060/ 0.090
Sn-doped InSe	0.082	56	0.060

(* N_a: concentrations of acceptor; N_d: concentrations of donor; E_c-E_d: ionization energy of the donor level.)

It is found that the conduction of pure InSe is dominated by the shallow donor level at 0.027 eV, while shallow donor levels of Ge and Sn doped InSe are at 0.09 eV and 0.06 eV below the conduction band, respectively. The results indicate that the presence of Ge, Sn is in shallow donor levels. Since the number of donors in InSe(Ge) and InSe(Sn) is greater than that of the pure InSe, acceptors that exist in the pure InSe have been electrically compensated. Carriers in these shallow states could be easily excited into the conduction band contributing to the photocurrent. Meanwhile, it takes a longer time for these trapped carriers to reach thermal balance.

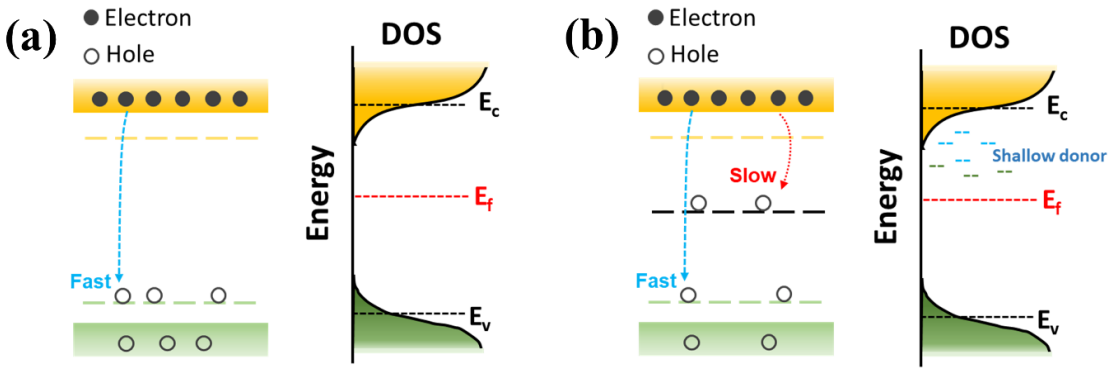

Figure 3. Simplified energy band diagram of (a) pure InSe and (b) doped-InSe showing valence and conduction bands, Fermi level, and shallow donor levels within the bandgap.

Firstly, to evaluate the quality of as-prepared samples, current-voltage (I-V) curves of pure InSe, InSe(Ge) and InSe(Sn) single crystals were measured in the dark and under light exposure. It should be noted that prior to optoelectrical measurements, all of the samples were stored in a dark environment overnight to ensure complete relaxation. Narrow band LED lights were used as light sources, including IR 980 nm (1.26 eV), red 620 nm (2.00 eV), green 516 nm (2.40 eV) and blue 460 nm (2.70 eV). **Figure 4**a displays I-V characteristics under chosen light wavelengths at a fixed light power of 0.3 mW. For the detailed IV plots information, see **Figure S4**. I-V curves are linear and symmetric in -1 V to 1 V bias regions, demonstrating ohmic

contact was assured between measured samples and Cr/Au electrode. It is observed that an exceptionally greater photocurrent has been attained for pure InSe, InSe(Ge), and InSe(Sn) photodetector under red LED in comparison with the other light sources. This is expected since the absorption edges of InSe, InSe(Ge), and InSe(Sn) are closed to red light excitation energy. The photocurrent for the emission energy close to the energy band shows more effective excitation from the valence band and/or defect (impurity) level to the conduction band. Ge, Sn dopants introduce impurities into the forbidden band, which are additional electronic occupied states; these multiple levels provide electrons with transit state entering conduction band. Note that InSe(Sn) achieved a maximum photocurrent value of 3.4×10^{-5} A at 1 V, which is enhanced up to 14 times than that of InSe(Ge) and 10^3 times than that of pure InSe.

For further investigating the mechanism behind the photocurrent generation, the relationship between the photocurrent and the light power intensity was fitted in Figure 4b using the power law equation $I \sim p^{\alpha}$,[28],[29] where p and α represent the light power intensity and the index of the power-law, respectively. Under the red LED, the maximum photocurrent can be extracted from each value of light intensity corresponding to 1.27 mW cm^{-2} ~ 38.20 mW cm^{-2}, and the three datasets correspond to the three cases of the samples (black dot: pure InSe, red dot: InSe(Ge), blue dot: InSe(Sn)). The results show that the three fitting curves sub-linearly respond to the light power, indicating that photocurrent and the light power intensity coincide with the power law. Theoretically, for a trap-free semiconductor, the efficiency of photogenerated charge carriers is proportional to the absorbed photon, so the ideal exponent α value should be equal to 1.[30][31] Interestingly, it is noted that the α value is characterized as 0.27 for InSe(Sn), which is bigger than that of InSe(Ge) and pure InSe. Moreover, the index of the power-law for three samples deviated from the ideal value, which accounts for dopant states in the semiconductor.[32][33] We speculate this is related to the extrinsic and intrinsic defects, including the In vacancy (V_{In}) and the Se vacancy (V_{Se}). V_{In} is a deep acceptor and V_{Se} is an electrically neutral defect, which cannot offer electrons (or holes), thus they may trap and localize photoexcited carriers. On the other hand, apart from V_{In} and V_{Se}, Ge-doping and Sn-doping create shallow donor levels below the conduction band in the doped InSe crystals. Ge- and Sn-impurities make electrical compensation and enhance light power density sensitivity.

Another charge transport feature exhibited by doped InSe is shown in Figure 4c. Dark current was measured from -1 V to 1 V. One can see that the current leakage increased significantly after doping, with the increased ratio of 7.6 orders for InSe(Ge) and 200 orders for InSe(Sn) at 1 V. We attribute the increment in dark current for Ge-, Sn- doped cases is a major contribution

from impurity-assisted generated charges, schematically depicted in Figure 4d. Additionally, the ideal factor can be extracted from the dark I-V curve following the diode current equation:

$I = I_s \times [\exp(qV/nKT) - 1]$,[34]

where I_s is the saturation current, q is the electronic charge (1.6×10^{-19}), V is the applied voltage, n is the ideal factor, k is the Boltzmann constant (1.38×10^{-23} m^2 kg s^{-2} K^{-1}), and T is the absolute temperature. The n value stands for two types of current: when the n value is less than 2, the current is close to the diffusion current; otherwise, the current stems from the combination current. Pristine InSe doped by Ge and Sn, the slope of the current increases from 1.68 to 1.72, which means that the current is close to the diffusion current after doping due to the compensation for native defects by extrinsic dopants.

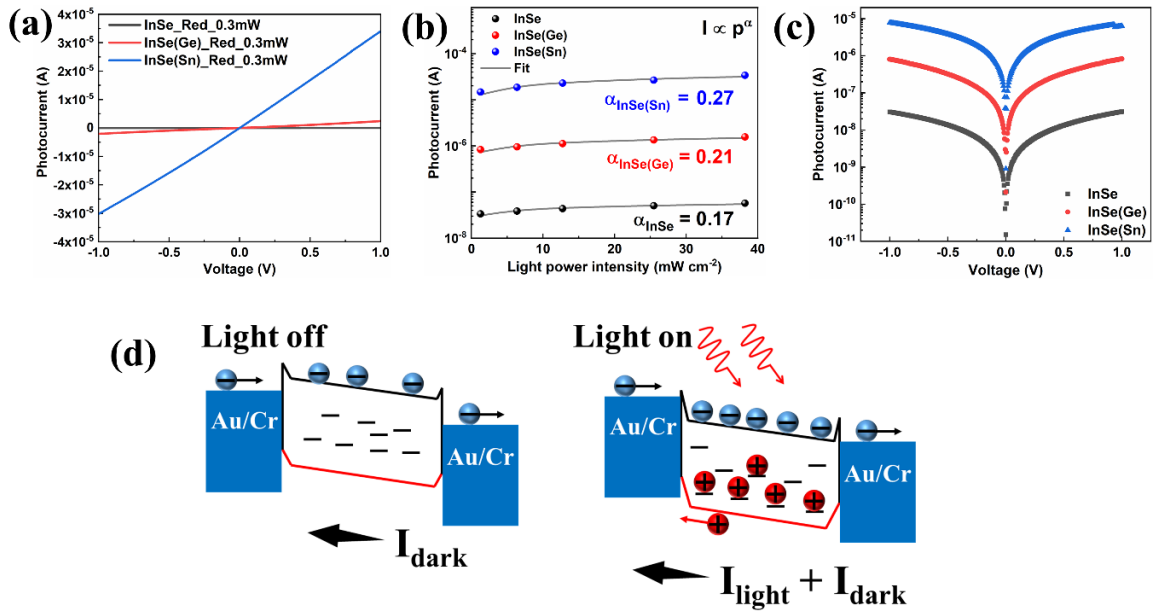

Figure 4. Current-voltage characteristics of pure InSe, InSe(Ge), and InSe(Sn) (a) Under red LED exposure; (b) Measured and fitted photocurrent; (c) Dark condition; (d) Band alignment for a semiconductor channel with two Au contacts under external bias in dark condition and upon illumination.

Based on the I-V measurements discussed above, here we also analyzed the current-time (I-t) performance of pure, InSe(Ge) and InSe(Sn) photodetectors for various LEDs illumination at 0.3 mW (**Figure S4**, Supporting Information). Cases of pure InSe and doped InSe maintain the highest photocurrent upon the red LED. Pure InSe-based photodetector exhibits a sharp rising/fall switching in the photocurrent during the periodic on/off cycle under different light sources. In contrast, InSe(Ge) and InSe(Sn) photodetectors go followed by the slower dynamics

of the increase in the photocurrent with subsequent slow relaxation to the initial dark current. This phenomenon verifies that extrinsic dopants are responsible for obvious PPC rather than the native defects (In vacancy and Se vacancy) in pure InSe. Apparently, the excited persistent photoconductivity in both doped InSe samples could be triggered by sub-bandgap irradiations. So, the photo-responsible Ge, Sn impurities are mainly concentrated on 2 eV above the valence band corresponding to the red band region. A similar defect level dependence of excitation energy could be observed in single crystal ZnO bulk.[35]

To better understand the mechanism of persistent photoconductive behavior induced by extrinsic impurity, we analyzed the case of PPC phenomena based on the red LED illumination, shown in **Figure 5**a. Compared to the pure InSe, the remarkable enhancement in photocurrent of 10^3 times for InSe(Sn); 65 times for InSe(Ge) have been recorded. The absence of the PPC effect in the pure InSe sample clearly demonstrated that the decay time was caused by the extrinsic dopant. Since the introduction of Ge, Sn dopants cause additional shallow donor levels in the forbidden band, electrons in these impurities state easily transit to the conduction band exposure on the radiation. In addition, increased photoexcited carrier concentrations may contribute to the photocurrent. So, it is anticipated that photocurrent is enhanced when Ge, Sn are doped in InSe.

For a photodiode, the rise time is defined as the time from 10 to 90% of rising photocurrent, otherwise, the time from 90 to 10% of falling photocurrent is fall time. In general, photogenerated electron-hole pairs could be quickly separated, and then electrons jump into the conduction band; the remaining holes move towards the corresponding electrode to form photocurrent.[36] Here, the persistent conductivity is evident in InSe(Ge) and InSe(Sn) photodetectors, but not in pure InSe-based photodetector. The pure InSe shows fast photocurrent decay after the cessation of a light source, which stems from the fact that the electron-hole pairs follow the fast direct band recombination. While, the photocurrent for Ge-Sn doped samples exhibits a prolonged decay within millisecond time scale after the light cut-off, namely the rise and fall periods of Ge-, Sn-doped InSe are longer than those of undoped InSe. These localized states introduced by dopants are shallow traps closed to the conduction band since pure InSe, InSe(Ge) and InSe(Sn) are reported as *n*-type semiconductors.

The observed PPC can be illustrated by the energy band diagram shown in Figure 3. Upon photoexcitation, electrons are excited from the valence band to the conduction band, forming photoconductivity. In this process, part of the carriers will be bounded by the defect (impurity)

states. These bounded carriers have two destinations: I. directly quenching by ionized defects (impurities); II. overcoming the captured barrier with sufficient kinetic energy to be re-excited. According to the preliminary experiment results, for intrinsic InSe, electrically neutral Se vacancy is formed easily, while vacancy is a deep acceptor with high formation energy. However, situations are different when Ge-, Sn- doped into intrinsic InSe. Specifically, Sn interstitials to be shallow donor dopant with ionization energy of 0.044 eV and donor level at 0.060 eV below the conduction band, whereas Ge and Se substitutional impurities act as donor-acceptor recombination.[25]-[27] It should be noted that, when both shallow and deep traps mutually exist in semiconductors, the deeper ones are firstly filled in by photoexcited electrons (holes) under light illumination.[37][38] Therefore, we attribute the PPC in the doped InSe to Ge, Sn interstitial impurities (extrinsic defects). In this respect, it is easy to explain photocurrent of InSe(Ge) and InSe(Sn) are better than InSe; both doped InSe cases show a similar delay time in the PPC.

Subsequently, we chose the red LED as the excitation source for investigating the PPC based on InSe(Sn) photodetector in detail. Figure 5b shows the temporal evolution of the current-time (I-t) in ambient conditions at room temperature. The fast response of the current (stage 2) appeared from the dark current (stage 1) after light excitation. This process is attributed to the conducting electrons and holes follow a band-to-band transition. Then the current (stage 3) slowly increased to reach a value over 100 times of magnitude above the dark current. After the irradiation was terminated, photoconductivity decay has two general components: firstly, a fast decay (stage 4) because of the band-to-band recombination, followed by slow decay (stage 5). The slow decay component is noticeable PPC relaxation, and residual photoconductivity will persist for a long time.

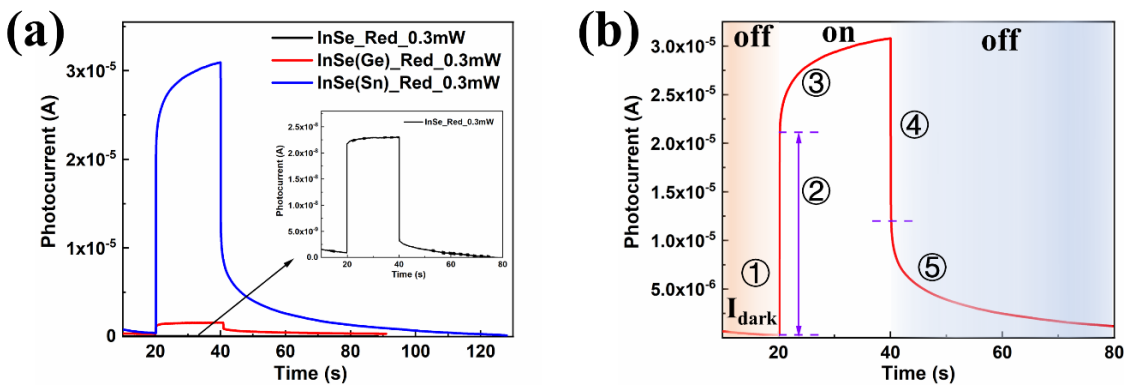

Figure 5. (a) Persistent photoconductivity curves for pure InSe, InSe(Ge), and InSe(Sn) upon

red LED. (b) Single photoresponse of InSe(Sn) device that includes 5 stages.

Next, we present the time dependence on the photon-induced current further to validate the PPC in our doped InSe samples. **Figure 6**a, b show the time evolution of photocurrent rise and decay, in which PPC increases with the excitation power and all light-intensities are well fitted by the stretch-exponential model.[39]

$\Delta I=I_s\{1-\exp[-(t/\tau_{ex})^{ßex}]\}$,

where I_s is the saturation current of light excitation, τ_{ex} represents the time constant upon light excitation, and β_{ex} is the stretch-exponent upon light excitation. The PPC recovery process goes as follow:

$\Delta I =I_0\{\exp[-(t/\tau_{re})^{ßre}]\}$,

where I_0 is the initial current value of light cutting off, τ_{re} is the recovery time constant, and β_{re} is the stretch-exponent of recovery.

As expected, the amplitude of the persistent photoconductivity increases as the excitation energy increases. It means the shortened carrier lifetime is accompanied by the increase in density of free carriers with the increased incident light power, which is consistent with previous reports.[3][7] In detail, the feature of the plots is similar at different light intensities: the photoconductivity initially rises rapidly, then tends to be slower before reaching a steady-state value under the illumination, and then a fast fall of current before long-term relaxation when switching off the illumination. In the exciting process under higher photon doses, more electrons and holes redistribute to occupy the local potential states before relaxing to the conduction band minimum (CBM) and valence band maximum (VBM). This redistribution slows down the relaxation of carriers, resulting in an extended τ after the illumination switch-off. Similar results were observed in the case of ReS_2, MoS_2 TI_6SeI_4.[40]-[42]

τ_{ex} and τ_{re} for the photoexcitation process (Figure 6c) and β_{ex} and β_{re} for the PPC recovery process (Figure 6d) dependence on the various red light intensity are extracted. Constant τ caused by defects (impurities) is determined by the time required for photoexcited electrons (hole) to escape from the trapped states, i.e. empty traps, deep level defect, shallow level defect. One can see that the τ_{ex} value is smaller than the $\tau_{re,}$ indicating that the electrons trapped process is faster than electrons release. Both β_{ex} and β_{re} increase as the light intensity and β_{ex} is much larger than β_{re}, indicating the distribution of traps in the recovery process is wider than in the photoexcitation process.[39]

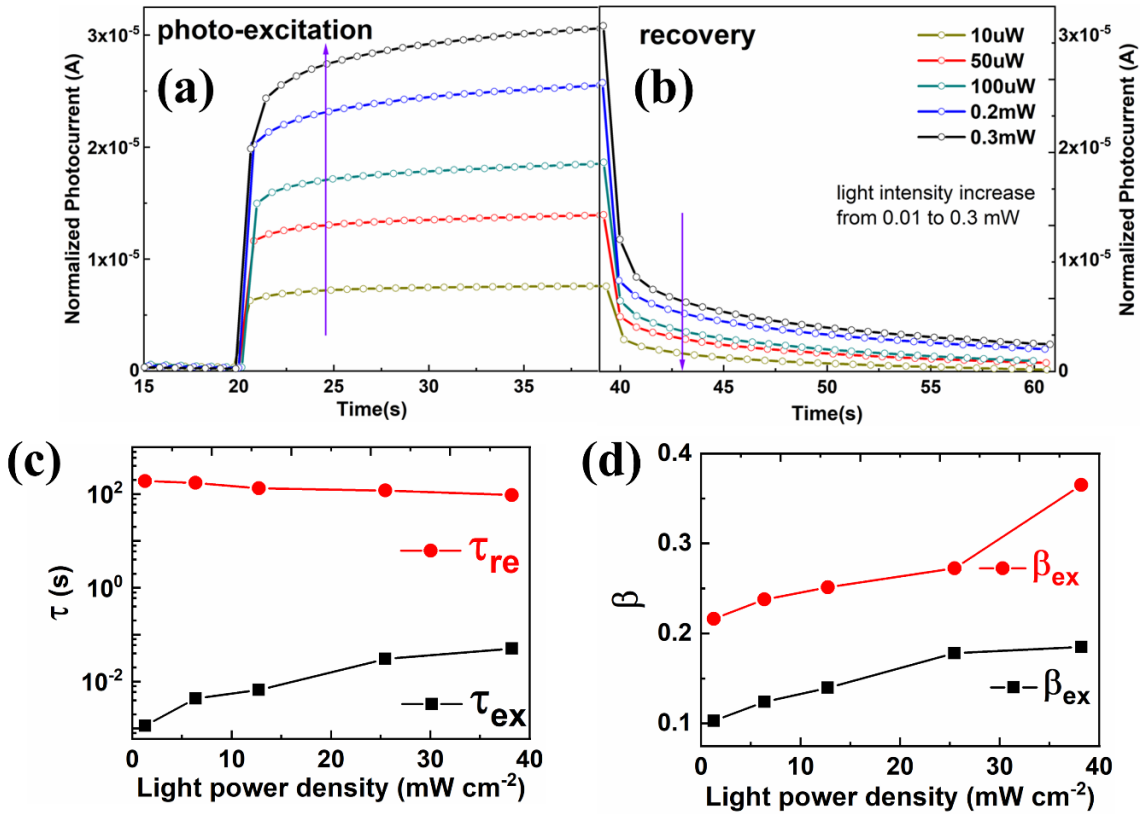

Figure 6. The time-dependent photo-induced current of InSe(Sn) under red LED (a) Photo-excitation and (b) Recovery stages, and solid lines are fitting curves; (c) Light intensity dependence of constant τ; (d) Stretch-exponent constant β.

In order to further study the impact of light intensity on Ge, Sn in pure InSe, the responsivity (R) and external quantum efficiency (EQE) as a function of light intensity upon red LED have been recorded in **Figure 7**a, b, respectively.

Their formula are:

$R = I_{ph}/ps\ (A\ W^{-1})$ [43]

$EQE(\lambda) = hcR/\lambda e$, [44]

where I_{ph} is photocurrent; p is the light power density and s is the effective illumination area; *h* is Planck's constant, *c* is the speed of light, λ is the wavelength of the incoming light, and *e* is the elementary charge.

In all cases, both R and EQE exhibit a negative dependence on the light intensity, reflecting the typical feature of layered material based on photodetectors.[45][46] The responsivity of InSe(Sn) reaches up to 1.7×10^6 W A^{-1} at 1.27 mW cm^{-2}, which is 4×10^2 times better than the pure InSe. The maximum EQE is up to 3.2×10^6 at 1.27 mW cm^{-2} for InSe(Sn), and the EQE value for

InSe(Ge) is also higher as compared to the pure one, indicating Ge, Sn doping could improve the light-to-current conversion of intrinsic InSe.

Another key figure of merit detectivity D* is calculated in **Figure 7**c. It can be calculated by the following equation[47] $D^* = R \times (S)^{0.5}/(e \times I_{off})^{0.5}$, where q and I_{off} are elementary charge and dark current, respectively. InSe(Sn) shows the best capability to distinguish weak optical signals. Here it is important to mention that the detectivity of InSe(Sn) obtained a higher detectivity value compared to other photodetectors. Further comparison with some of the typical photodetectors is summarized in **Table S1** (Supporting Information).

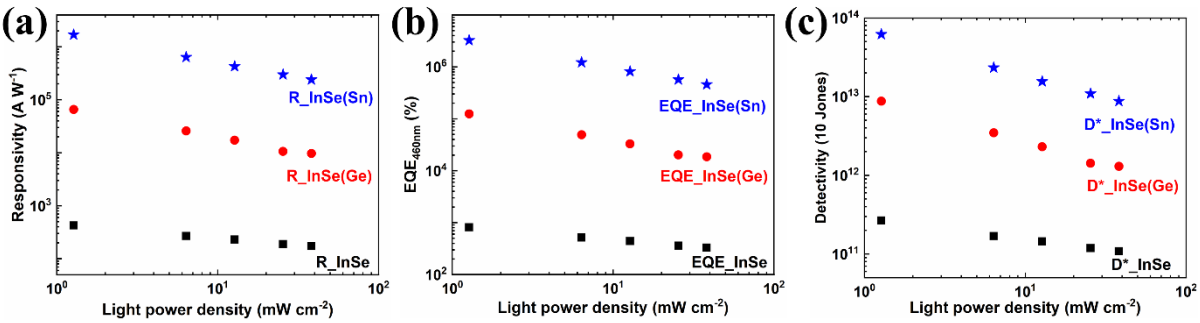

Figure 7. Illumination dependence (a) responsivity (R); (b) external quantum efficiency (EQE); and (c) detectivity (D*) of as-prepared pure InSe, InSe(Ge) and InSe(Sn) photodetector measured under the applied bias of 1 V.

The aforementioned experiments discussed aimed at energetic characterization and optoelectrical performance of the persistent photoconductivity. In the following part, we explored the effect of hall mobility and carrier density on persistent photoconductivity. So, we carried on Hall effect measurements on pure InSe, InSe(Ge) and InSe(Sn) samples. The carrier concentrations were determined based on the formula: $n = -B_z I_x/dV_H e$, where B_z is the magnetic field, I_x is the electric current, d is the sample thickness, V_H is the Hall voltage, e is the charged electron. Based on the data in **Table 2**, we observe a reduced trend in carrier concentration for InSe(Ge) and InSe(Sn) cases compared with pure InSe. The reduced carrier concentration in doped InSe can be explained by the dopants, which serve as charge carrier scattering centers. The persistent photoconductivity is thus partly caused by a decrease in carrier density. Hall mobility in our case is determined by dopant scattering. One can see that enhancement of hall mobility for InSe(Ge) case (880.04 $cm^2V^{-1}s^{-1}$) and InSe(Sn) case (754.85 $cm^2V^{-1}s^{-1}$) compared with the pristine InSe (648.64 $cm^2V^{-1}s^{-1}$). The hall mobility in our case is determined by ionized impurity scattering. The increased Hall mobility reflects the increase of barrier height caused by the capture of photogenerated electrons, so we could observe the obvious PPC in the doped

InSe samples.

Table 2. Hall measurement parameters of the pure InSe, InSe(Ge) and InSe(Sn) samples.

Sample	Carrier Concentration [cmA^{-3}]	Hall Mobility [$cm^2V^{-1}s^{-1}$]	Sheet Resistance [Ω cm]
InSe	1.64×10^{16}	684.64	6.48
InSe(Ge)	2.7×10^{15}	880.04	3.83
InSe(Sn)	1.48×10^{15}	754.85	4.5

3. Conclusion

In summary, we have synthesized high-quality pure InSe and Ge-, Sn-doped InSe single crystals and investigated their optoelectrical properties. A systematic study of persistent photoconductivity and optoelectrical performance in pure InSe and InSe(Ge), InSe(Sn) bulk single crystals photodetector was performed. Persistent photoconductivity at room temperature has been observed in Ge-, Sn-doped InSe, and the PPC effect increases as the higher light intensities and photon doses. These results reveal that Ge, Sn impurities form shallow donor levels in the pure InSe, which promote the excitation of electrons from dopant levels to the conduction band. Meanwhile, the presence of these shallow states contributes to the relaxation of photoconductivity. Dopant-assisted generated photoconductivity is responsible for the improved photocurrent of InSe(Sn) and InSe(Ge) by 10^3 and 14 orders of magnitude, respectively. Additionally, Hall effect measurements allow us to distinguish between hall mobility and charge carrier effects on Ge and Sn dopants. Our results can boost the potential application of resistive switching materials, offering opportunities to photoconductivity and detectivity properties for burgeoning photoelectrical memory devices.

4. Experimental Section

4.1 Crystals growth

Crystals used in the aforementioned experiment were grown by the conventional Bridgman technique. The pure InSe crystal growth was in a non-stoichiometric melt 52 at.% of In and 48 at.% of Se. High-purity In (6N; granules) and Se (6N; granules) from Wuhan Xinrong New

Materials, Co. Ltd. were placed in a quartz glass ampoule and melt-sealed under high vacuum (below $1x10^{-3}$ Pa). The ampule with melted reaction mixture was heated at 800 °C for 12 h, going follow cooling down at the rate of 0.1 °C min^{-1}. Ge-doped InSe and Sn-doped InSe crystals were grown in the same procedures described above. ICP-OES shows a concentration of 676 ppm of tin, 186 ppm of germanium, respectively. As-prepared crystals were stored in a glovebox.

4.2 Characterizations

The crystal structures were analyzed by X-ray diffraction with a Bruker D8 Discoverer powder diffractometer in Bragg- Brentano geometry. The diffraction patterns were collected from 5-90° with a step of 0.02 (Cu Kα radiation; λ = 0.15418 nm, V = 40 kV, I = 40 mA). Morphological and elemental analyses were carried out by scanning electron microscopy (JEOL 7600F, Japan) with X-MaxN 80 T detector (Oxford Instruments, Great Britain) for SEM-EDS measurement. The Raman and photoluminescence spectra were measured on an inVia Raman microscope (Renishaw, Great Britain) with a charge-coupled device detector. Samples were placed on the silicon wafer, and 20× objective, laser power of 5 mW, and exposure time of 20 s were employed. The UV-Vis measurements were carried out on PerkinElmer LAMBDA 850. Hall-effect measurements were characterized using DX-100 Hall Effect System (Dexing Magnet Tech. Co., Limited). Samples were measured at room temperature on a four-point probe placed between the plates of an electromagnet based on the van der Pauw configuration. Other condition parameters are as follows: the current measuring range is 10 mA (d.c.), and the magnetic field is 0.5 T.

4.3 Device fabrication and measurement

Photodetectors in the experiment were constructed based on single crystals. Firstly, Si/SiO_2 wafer was cleaned by sonication using acetone, methanol, and dilute water for 15 min in successive. Then, the InSe, Ge-doped InSe, Sn-doped InSe single crystal were constructed on the Si/SiO_2 substrate respectively, covered with transmission electron microscope (TEM) grid as a shadow mask. Au electrodes (5 nm Cr/40 nm Au) were thermally evaporated on top of crystals, and the channel width between two Au contacts is 37 μm.

The photodetection properties were measured using a homemade probe station with Keysight B2902A semiconductor characterization system. Fiber-coupled LED (Thorlabs-M470F3) was used to supply the illumination, and LED controller (Thorlabs, LEDD1B) adjusted the light power. A silicon photodiode calibrator was used to calibrate the light power density.

Supporting Information: Supporting Information is available from the Wiley Online Library or from the author.

Acknowledgment This work was supported by project LTAUSA19034 from Ministry of Education Youth and Sports (MEYS). Ph.D. students were supported by specific university research (MSMT No. 20-SVV/2022). L.L.P gratefully acknowledges the financial support of the China Scholarship Council (CSC) (No. 202108160003).

Conflict of Interest The authors declare no competing financial interest.

References

[1] H. Wang, D. H. Kim, *Chemical Society Reviews* **2017**, 46, 5204.

[2] S. Sze, K. K. Ng, *Physics of Semiconductor Devices* **2006**, 3, 601.

[3] S. McGlynn, *Journal of the American Chemical Society* **1964**, 86, 5707.

[4] R. H. Bube, *Photoconductivity of solids*, Wiley, New York **1960**.

[5] F. H. Koppens, T. Mueller, P. Avouris, A. C. Ferrari, M. S. Vitiello, M. Polini, *Nature Nanotechnology* **2014**, 9, 780.

[6] H. Fang, W. Hu, *Advanced Science* **2017**, 4, 1700323.

[7] Z. Chen, X. Li, J. Wang, L. Tao, M. Long, S. J. Liang, L. K. Ang, C. Shu, H. K. Tsang, J. B. Xu, *ACS Nano* **2017**, 11, 430.

[8] B. G. Streetman, *Journal of Applied Physics* **1966**, 37, 3137.

[9] Y. Z. Guo, J. Robertson, *Physical Review Materials* **2017**, 1, 044004.

[10] L. P. Liao, Y. Q. Yao, G. Wang, C. Y. Xu, D. B. Liu, G. D. Zhou, Y. X. Zhong, Q. L. Song, *Journal of Cleaner Production* **2021**, 278, 124168.

[11] X. P. Li, C. X. Xia, J. Du, W. Q. Xiong, *Journal of Materials Science* **2018**, 53, 3500.

[12] S. Shigetomi, T. Ikari, *Journal of Applied Physics* **2000**, 88, 1520.

[13] J. Martínez-Pastor, A. Segura, J. L. Valdés, A. Chevy, *Journal of Applied Physics* **1987**, 62, 1477.

[14] Q. H. Zhao, W. Wang, F. Carrascoso-Plana, W. Q. Jie, T. Wang, A. Castellanos-Gomez, R. Frisenda, *Materials Horizons* **2020**, 7, 252.

[15] A. Segura, J. P. Guesdon, J. M. Besson, A. Chevy, *Journal of Applied Physics* **1983**, 54, 876.

[16] S. S. Choo, S. W. Hong, H. S. Kim, S. I. Kim, *Korean Journal of Metals and Materials* **2020**, 58, 348.

[17] W. Zhu, T. Low, Y. H. Lee, H. Wang, D. B. Farmer, J. Kong, F. Xia, P. Avouris, *Nature Communications* **2014**, 5, 3087.

[18] H. Qiu, T. Xu, Z. Wang, W. Ren, H. Nan, Z. Ni, Q. Chen, S. Yuan, F. Miao, F. Song, G. Long, Y. Shi, L. Sun, J. Wang, X. Wang, *Nature Communications* **2013**, 4, 2642.

[19] S. Ghatak, A. N. Pal, A. Ghosh, *ACS Nano* **2011**, 5, 7707.

[20] J. F. Sánchez-Royo, G. Muñoz-Matutano, M. Brotons-Gisbert, J. P. Martínez-Pastor, A. Segura, A. Cantarero, R. Mata, J. Canet-Ferrer, G. Tobias, E. Canadell, J. Marqués-Hueso, B. D. Gerardot, *ACS Nano* **2011**, 7, 1556.

[21] J. Tauc, *Materials Research Bulletin* **1968**, 3, 37.

[22] F. J. Manjón, A. Segura, V. Muñoz-Sanjosé, G. Tobías, P. Ordejón, E. Canadell, *Physical Review B* **2004**, 70, 125201.

[23] S. R. Weng, W. L. Zhen, Y. D. Li, X. Yan, H. Han, H. Huang, L. Pi, W. K. Zhu, H. Li, C. J. Zhang, *Physica Status Solidi-Rapid Research Letters* **2020**, 14, 2000085.

[24] W. Yang, B. Liu, T. Fang, W. A. Jennifer, L. Christophe, Z. Li, X. Zhang, X. Jiang, *Nanoscale* **2016**, 8, 18197.

[25] S. Shigetomi, T. Ikari, *Journal of Applied Physics* **2003**, 93, 2301.

[26] S. Shigetomi, T. Ikari, *Physica Status Solidi B-Basic Research* **2003**, 236, 135.

[27] D. Wang, X. B. Li, H. B. Sun, *Nanoscale* **2017**, 9, 11619.

[28] Q. H. Zhao, R. Frisenda, P. Gant, D. P. De Lara, C. Munuera, M. Garcia-Hernandez, Y. Niu, T. Wang, W. jie, A. Castellanos-Gomez, *Advanced Functional Materials* **2018**, 28, 1805304.

[29] O. Lopez-Sanchez, D. Lembke, M. Kayci, A. Radenovic, A. Kis, *Nature Nanotechnology* **2013**, 8, 497.

[30] Z. Wang, M. Safdar, M. Mirza, K. Xu, Q. Wang, Y. Huang, F. Wang, X. Zhan, J. He, *Nanoscale* **2015**, 7, 7252.

[31] H. Kind, H. Q. Yan, B. Messer, M. Law, P. D. Yang, *Advanced Materials* **2002**, 14, 158.

[32] K. Kannan, D. Radhika, A. S. Nesaraj, M. Wasee Ahmed, R. Namitha, *Materials Research Innovations* **2020**, 24, 414.

[33] W. W. Tsai, Y. C. Chao, E. C. Chen, H. W. Zan, H. F. Meng, C. S. Hsu, *Applied Physics Letters* **2009**, 95, 213308.

[34] C. C. Yang, P. H. Chen, T. C. Chang, W. C. Su, S. Y. Chen, S. C. Liu, S. Y. Chou, Y. F. Tan, C. C. Lin, P. Y. Wu, T. M. Tsai, H. C. Huang, *Nanoscale Research Letters* **2019**, 14, 375.

[35] K. Kuriyama, K. Matsumoto, Y. Suzuki, K. Kushida, Q. Xu, *Solid State Communications* **2009**, 149, 1347.

[36] D. Wu, Y. Jiang, Y. G. Zhang, Y. Q. Yu, Z. F. Zhu, X. Z. Lan, F. Z. Li, C. Y. Wu, L. Wang, L. B. Luo, *Journal of Materials Chemistry* **2012**, 22, 23272.

[37] G. Konstantatos, J. Clifford, L. Levina, E. H. Sargent, *Nature Photonics* **2007**, 1, 531.

[38] J. A. Hornbeck, J. R. Haynes, *Physical Review* **1955**, 97, 311.

[39] J. J. Luo, A. U. Adler, T. O. Mason, D. B. Buchholz, R. P. H. Chang, M. Grayson, *Journal of Applied Physics* **2013**, 113, 153709.

[40] S. Das, J. A. Peters, W. Lin, S. S. Kostina, P. Chen, J. I. Kim, M. G. Kanatzidis, B. W. Wessels, *Journal of Physical Chemistry Letters* **2017**, 8, 1538.

[41] J. Jiang, C. Ling, T. Xu, W. Wang, X. Niu, A. Zafar, Z. Yan, X. Wang, Y. You, L. Sun, J. Lu, J. Wang, Z. Ni, *Advanced Materials* **2018**, 30, e1804332.

[42] Y. C. Wu, C. H. Liu, S. Y. Chen, F. Y. Shih, P. H. Ho, C. W. Chen, C. T. Liang, W. H. Wang, *Scientific Reports* **2015**, 5, 11472.

[43] Y. Yang, X. Wang, S. C. Liu, Z. Li, Z. Sun, C. Hu, D. J. Xue, G. Zhang, J. S. Hu, *Advanced Science* **2019**, 6, 1801810.

[44] J. Yao, G. Yang, *Nanoscale* **2020**, 12, 454.

[45] X. Wen, Z. Lu, L. Valdman, G. C. Wang, M. Washington, T. M. Lu, *ACS Applied Materials & Interfaces* **2020**, 12, 35222.

[46] X. Wang, P. Wang, J. Wang, W. Hu, X. Zhou, N. Guo, H. Huang, S. Sun, H. Shen, T. Lin, M. Tang, L. Liao, A. Jiang, J. Sun, X. Meng, X. Chen, W. Lu, J. Chu, *Advanced Materials* **2015**, 27, 6575.

[47] L. H. Zeng, S. H. Lin, Z. J. Li, Z. X. Zhang, T. F. Zhang, C. Xie, C. H. Mak, Y. Chai, S. P. Lau, L. B. Luo, Y. H. Tsang, *Advanced Functional Materials* **2018**, 28, 1705970.

Table of Contents

1. For the first time, a systematic study of excitation energy dependence on persistent photoconductivity in Ge-, Sn-doped InSe single crystal.

2. Ge and Sn dopants are responsible for shallow donor level in the pure InSe, which contributes to the relaxation of photoconductivity.

3. Optoelectronic measurements reveal the potential mechanism of dopant-assisted improved optoelectrical performance.